Elastohydrodynamic relaxation of soft and deformable microchannels

Gabriel Guyard, Frédéric Restagno, Joshua D Mcgraw

Elastohydrodynamic relaxation of soft and deformable microchannels

Gabriel Guyard,[1, 2, 3] Frédéric Restagno,[3] and Joshua D. McGraw[1, 2, *]

[1] *Gulliver CNRS UMR 7083, PSL Research University, ESPCI Paris, 10 rue Vauquelin, 75005 Paris, France*

[2] *IPGG, 6 rue Jean-Calvin, 75005 Paris, France*

[3] *Université Paris-Saclay, CNRS, Laboratoire de Physique des Solides, 91405, Orsay, France*

(Dated: July 11, 2022)

Hydrodynamic flows in compliant channels are of great interest in physiology and microfluidics. In these situations, elastohydrodynamic coupling leads to: (*i*) a nonlinear pressure-*vs.*-flow-rate relation, strongly affecting the hydraulic resistance; and (*ii*), because of the compliance-enabled volume storage, a finite relaxation time under a step-wise change in pressure. This latter effect remains relatively unexplored, even while the time scale can vary over a decade in typical situations. In this study we provide time-resolved measurements of the relaxation dynamics for thin and soft, rectangular microfluidic channels. We describe our data using a perturbative lubrication approximation of the Stokes equation coupled to linear elasticity, while taking into account the effect compliance and resistance of the entrance. The modelling allows to completely describe all of the experimental results. Our work is relevant for any microfluidic scenario wherein a time-dependent driving is applied and provides a first step in the dynamical description of compliant channel networks.

To force the movement of fluid through a narrow channel, a pressure drop must be applied between its entrance and exit. If the bounding walls of this simple flow domain are compliant, their pressure-induced deformation can strongly affect the flow as compared to the non-compliant case. This elastohydrodynamic coupling is often encountered, and the pipe-flow case is referred to as soft hydraulics [1]. Particularly, the flow modification can give a non-linear pressure-*vs.*-flow-rate relation [2, 3], with the flow resistance changing by an order of magnitude or more. Upon a pressure change, however, the relaxation to a new deformation profile is not instantaneous. The pipe thus settles into a new configuration over a little-investigated, pressure-dependent time scale that is the main focus of this Letter.

Elastohydrodynamics (EHD) was historically studied in the context of lubrication of rough, solid contacts [4–6], often for heavy mechanical applications and remains a key ingredient in modern tribology [7]. Conversely, the lubrication of soft materials has attracted increasing attention in the last decades [8–12] due in part to the relevance of the topic in biology and microtechnologies. Several important examples of the former class of problems include joint lubrication [13], eyelid wiper mechanics [14], and the deformation of blood vessels under flow-induced pressure [15–18] — the latter at stake, for example, in atherosclerosis [19]. At microscales, EHD interactions may affect the transport of blood cells [20] because of the emergent lift forces arising from the fluid-mediated soft-substrate deformation [21].

Concerning soft technologies, microfluidics is of significant interest [22]. Indeed, microchannels are typically made with soft elastomers —typically polydimethylsiloxane (PDMS)— since these materials are transparent, allow fast prototyping and are easily demolded with fidelity [23, 24]. Compliance is a key attribute for applications such as organ-on-a-chip [25, 26] or wearable technologies [27, 28]. Targeted actuation of deformable pipes also allows to generate and manipulate flows at the scale of a single channel [29–31], or in complex networks [32] as in the plant kingdom [33]. Finally, soft components can be used to make pressure-controlled valves serving as building blocks for the logic gate components that are key to state-of-the-art microfluidic devices [34–36].

While many soft-hydraulics-based studies focus on the steady state, compliance is also expected to have dynamic effects. This deformability leads to volume storage capacity [37], schematically indicated in Fig. 1(a), which in addition to changing the resistance of a narrow channel, implies a characteristic response time of the system by analogy with electronics [38, 39], see Fig. 1(b). This dynamic response was used for example to attenuate parasitic fluctuations in syringe-pump driven flows [40], and limits the production rate in stop-flow lithography [41].

With dynamical aspects of soft hydraulics already finding applications, it is imperative to systematically and quantitatively characterize the temporal response of compliant microchannels. Here we experimentally and theoretically investigate the response of thin, soft microfluidic channels to step-wise pressure perturbations. We use an EHD model in the lubrication limit applied to such devices. As previously [2, 3, 42], such an approach allows to rationalise the nonlinear relation between pressure and flow rate. Then, performing a perturbation analysis and, crucially, specifying the capacitance and resistance of the peripheral components, the pressure-dependent relaxation dynamics of the entire experimental system is revealed. Our approach includes an asymptotic analysis of the general high- and low-pressure limits, along with the full crossover requiring complete specification of the microsystem.

The microfluidic chips used here consisted of in-

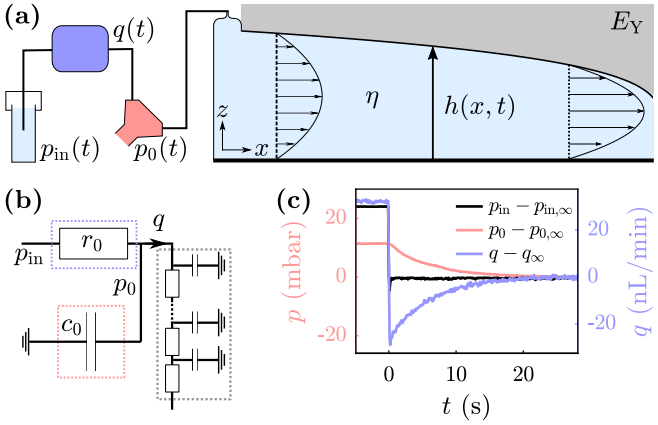

Figure 1. **(a)** Schematics of the microfluidic setup, including a flow sensor, a pressure sensor and a soft channel. **(b)** Equivalent electronic circuit, the flow sensor modelled with an ideal resistance r_0, the pressure sensor by a capacitance c_0, and the soft channel with a series of infinitesimal resistances and capacities. **(c)** Imposed p_{in} and measured p_0 and q as a function of t. The shifted, imposed pressure $p_{in,\infty} = 1301$ mbar, $p_{0,\infty} = 862$ mbar and $q_\infty = 1058$ nL/ min denote the long-time steady-state values of their associated signals.

let/outlet circles of radius $d_c = 1.0$ mm and rectangular channels with length $L = 4.0$ cm between the inlet/outlet centers. The channel widths were $w = \{200, 500, 1000, 2000\}$ µm, with uncertainty of order a few micrometers, and undeformed heights $h_0 = 5.0 \pm 0.1$ µm. The moulds were characterized with a mechanical profilometer (Bruker Dektak Stylus Profiler). Liquid reservoirs were connected to chips using plastic tubing with negligible hydraulic resistance and compliance (PEEK, IDEX 1581, ID 0.25 mm, OD 1/32" of typical length 50 cm). The microchannels were fabricated using standard soft lithography [43] from PDMS (Momentive RT 615 A & B) including 10 wt.% cross-linker, and cured at 170 °C for 15 minutes.

Flow and pressure sensors (Elveflow MFS1 and MPS2) provided time-resolved measurements of the flow rate q and pressure p_0, relative to atmospheric pressure, at the chip inlet. Ultra-pure water (Milli-Q, 18.2 MΩ cm, viscosity $\eta = 1.00 \pm 0.02$ mPa s) was driven using a pressure controller (Elveflow OB1 mk3+), with constant pressure, p_{in}, imposed across the input sensors and the microchannel, see Fig. 1(a). While the system is at steady state, p_{in}, was suddenly dropped by a constant amount, δp_{in}, and the responses $q(t)$ and $p_0(t)$ were recorded until a new steady state was reached; a selection of raw data is also shown in the Supplementary Material section S.I (SM, see Ref. [44]).

Figure 1(c) shows one set of recorded signals for $p_{in}(t)$, $p_0(t)$, and $q(t)$ after a sudden pressure drop. Each signal is shifted to its long time steady-state value, denoted $p_{in,\infty}$, $p_{0,\infty}$, and q_∞, respectively. Remarkably, while the imposed pressure p_{in} varied on a time scale of just 0.1 s, p_0 and q reach new steady states after a much longer transient time, of order 10 s, depending on the initial input pressure and channel geometry. In the following we study the dependence of q_∞ and τ_{exp} on $p_{0,\infty}$ and w.

In Fig. 2 is shown the scaled relation between the dimensionless flow rate Q_∞ and pressure $P_{0,\infty}$ for all of the chip geometries used here. While the raw data is shown in Supplemental Material [45], section S.II, here the pressure is normalized by the natural scale $p^* = E^* h_0/w$ with the semi-infinite slab case [2, 46] giving $E^* \approx E_Y/0.5427(1-\nu^2)$; ν and E_Y are the Poisson ratio and Young's modulus of the material [47]. The flow rate is normalized by p^*/r_c, with $r_c = 12\eta L/wh_0^3$ the hydraulic resistance of a rectangular channel [48]. Such a normalization gives a single master curve, and, in contrast to rigid pipe flow [48, 49], the flow-rate response of these channels is nonlinear for all the tested geometries. Indeed, when the pressure is increased the driving force increases; meanwhile the channel's resistance decreases due to its inflated geometry.

In Fig. 3 is shown $p_0 - p_{0,\infty}$ as a function of time in a 200 µm-wide channel for several $p_{0,\infty}$. Straight lines in semi-log axis suggest that the relaxation is exponential, with an experimental relaxation time τ_{exp}. Extracting this time with exponential fits, the inset of Fig. 3 shows τ_{exp} as a function of $p_{0,\infty}$. The relaxation time decreases by a factor of 5 across the accessible range of $p_{0,\infty}$. Since deformation allows the channel to store a pressure-dependent volume of fluid, the microfluidic chips used here are liquid-storage capacitors. The channels also exhibit resistance, so that they are essentially RC fluidic circuits [38, 48]. To quantitatively rationalize the nonlinearity of q_∞ with $p_{0,\infty}$, as well as the dependence of τ_{exp} on $p_{0,\infty}$, we propose the following elastohydrody-

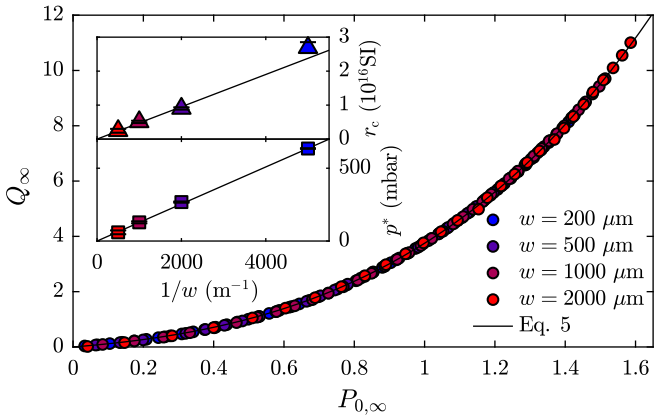

Figure 2. Dimensionless steady-state flow rate $Q_\infty = q_\infty r_c/p^*$ as a function of the dimensionless steady-state inlet pressure $P_{0,\infty} = p_{0,\infty}/p^*$ for soft and thin channels of different widths as indicated. The solid line indicates the model of Eq. 5. Error bars are smaller than symbol size. The fitting parameters p^* and r_c are shown in insets.

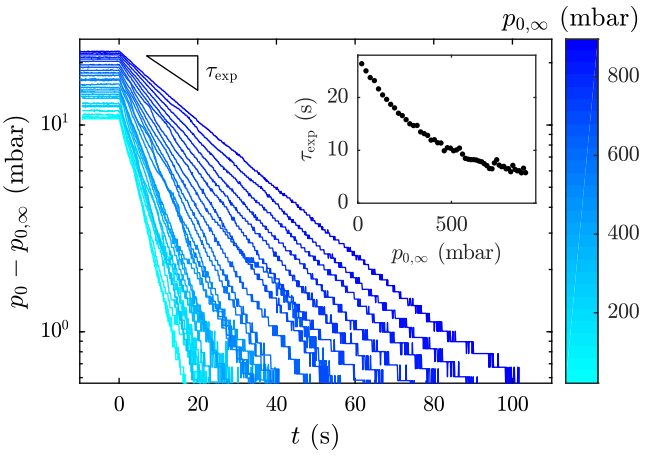

Figure 3. Experimental shifted inlet pressure $p_0 - p_{0,\infty}$ as a function of time t for the relaxation toward different steady states $p_{0,\infty}$, for a 200 µm-wide soft channel. The inset shows the measured relaxation time $\tau_{\rm exp}$, obtained by exponential fit of the data, as a function of $p_{0,\infty}$. Error bars are smaller than symbol size.

namic model.

Considering the one dimensional limit since $h_0 \ll w \ll L$, we denote $h(x,t)$ the time-dependent height of the microchannel along the center line and along the flow direction, x, and $p(x,t)$ the pressure field within the channel. In the lubrication limit, the Reynolds equation [50] expresses conservation of volume for incompressible, Newtonian fluids:

$$\partial_t h = \frac{1}{12\eta}\partial_x\left(h^3\partial_x p\right). \tag{1}$$

Since the former equation introduces the unknown fields $h(x,t)$ and $p(x,t)$, an elastic model is needed to connect the height profile to the pressure field. Even though the height profile varies in both the x and y directions as described in detail by Christov and coworkers [3, 42], we consider a local linear elastic response of the surrounding material along the center line:

$$h(x,t) = h_0 + \frac{w}{E^*}p(x,t)\ . \tag{2}$$

To close the problem, we consider the boundary condition at the outlet $p(L,t) = 0$. At the inlet, we need to account for the peripheral sensors. By analogy with electronics, the setup is described using the circuit depicted in Fig. 1(b). The flow sensor, composed of a thin hard glass capillary, is assumed an ideal resistance r_0. The pressure sensor, including deformable parts, is modelled with a negligibly-resistant capacity $c_0 = \mathrm{d}\Omega/\mathrm{d}p_0$ where Ω is the volume of fluid stored in the sensor. Flux conservation at channel inlet then reads:

$$\frac{p_{\rm in} - p_0}{r_0} - c_0\frac{\mathrm{d}p_0}{\mathrm{d}t} = \left(-\frac{wh^3}{12\eta}\partial_x p\right)\bigg|_{x=0}\ . \tag{3}$$

Non-dimensionalizing, we take: $h = h_0 H$, $x = LX$, $t = \tau_{\rm c} T$ with $\tau_{\rm c} = 12\eta w L^2/h_0^3 E^*$ as in Ref. [41], and pressures take the form $p = p^* P$. Then, combining Eq. 1 and Eq. 2, we obtain the elastohydrodynamic equation for the pressure field within the chip:

$$\partial_T P = \partial_X\left[(1+P)^3\,\partial_X P\right]. \tag{4}$$

In the steady state, with a constant inlet pressure $P_{0,\infty}$ and null outlet pressure, a single integration of Eq. 4 gives $P_\infty(X) = \left[(1-X)((1+P_{0,\infty})^4 - 1) + 1\right]^{1/4} - 1$. From this pressure profile, we compute the steady flux Q_∞ using the square-bracketed term of Eq. 4:

$$Q_\infty = \frac{1}{4}\left[(1+P_{0,\infty})^4 - 1\right] = \frac{1}{4}\Pi\ , \tag{5}$$

having introduced $\Pi = (1+P_{0,\infty})^4 - 1$. Equation 5 has a similar form to the expressions given previously [3, 42]. The data of Fig. 2 show excellent agreement with this model for all the tested chips, and for channel-height variations up to 160%. The fitting parameters for each chip, p^* and $r_{\rm c}$, follow the expected scaling with w, as can be seen in the insets. The slope of the straight line of the bottom inset provides a measurement of $E^* = 2.62 \pm 0.06$ MPa. This corresponds to $E_{\rm Y} = 1.07 \pm 0.03$ MPa which is consistent with the typical value for this PDMS.

Addressing the time-dependent problem, we linearize Eq. 4, introducing $\delta P(X,T) = P(X,T) - P_\infty(X)$. At $\mathcal{O}(\delta P^1)$ and after the change of variables $\tilde{X} = \Pi(1-X)$ and $\tilde{T} = \Pi^2 T$, we obtain:

$$\partial_{\tilde{T}}\delta P = \partial^2_{\tilde{X}}\left[\tilde{X}^{3/4}\delta P\right]. \tag{6}$$

Looking for separable solutions of Eq. 6, we propose $\delta P(\tilde{X},\tilde{T}) = A(\tilde{X})B(\tilde{T})$. Using the boundary condition for $\delta P = 0$ at $\tilde{X} = 1$, we obtain $B_\lambda(\tilde{T}) = \exp(-\lambda\tilde{T})$, confirming the experimentally observed exponential pressure decay; it remains to determine the allowed values of λ. Considering the spatial part, we have [51] $A_\lambda(\tilde{X}) = \alpha_\lambda\tilde{X}^{-1/4}\mathcal{C}_{\frac{4}{5}}\left(\frac{8\sqrt{\lambda}}{5}\tilde{X}^{5/8}\right)$, where α_λ is an integration constant. The function $\mathcal{C}_\nu$ is a linear combination of Bessel functions, here of the form $\mathcal{C}_\nu(x) = \mathrm{Y}_{\frac{4}{5}}\left(\frac{8\sqrt{\lambda}}{5}\right)\mathrm{J}_\nu(x) - \mathrm{J}_{\frac{4}{5}}\left(\frac{8\sqrt{\lambda}}{5}\right)\mathrm{Y}_\nu(x)$, satisfying the boundary condition at the channel exit.

For the boundary condition at the channel entrance, the full solution $P_\infty + \delta P(\tilde{X},\tilde{T})$ can be injected into the dimensionless version of Eq. 3. Such a substitution gives a constraining equation on the eigenvalues, λ, after evaluation at $\tilde{X}_0 = 1 + \Pi$:

$$\frac{1}{\mathcal{R}\tilde{X}_0^{3/8}}\left(\mathcal{T}\sqrt{\lambda}\Pi - \frac{1}{\sqrt{\lambda}\Pi}\right) = \frac{\mathcal{C}_{-\frac{1}{5}}\left(\frac{8\sqrt{\lambda}}{5}\tilde{X}_0^{5/8}\right)}{\mathcal{C}_{\frac{4}{5}}\left(\frac{8\sqrt{\lambda}}{5}\tilde{X}_0^{5/8}\right)}\ , \tag{7}$$

where we introduced $\mathcal{R} = r_0/r_{\rm c}$ and $\mathcal{T} = \tau_0/\tau_{\rm c}$. Recalling that the experimentally measured pressure relaxations of

Fig. 3 are well described by simple exponential decays, and if λ_s denotes the smallest allowed value of λ satisfying Eq. 7, the experimentally measured time scale is then assumed to be

$$\frac{\tau_{\rm exp}}{\tau_c} = \frac{1}{\Pi^2}\lambda_s^{-1}(\Pi, \mathcal{R}, \mathcal{T}) \ . \tag{8}$$

This relation shows that the relaxation time scale is a function of the pressure through Π, and in particular depends on the details of the input resistance and capacitance, here reflected through the dimensionless $\mathcal{R}$ and $\mathcal{T}$.

To the best of our knowledge, there is no analytic solution for λ_s through Eq. 7; nevertheless, the asymptotic behavior can be assessed. At low pressure, there is no significant channel deformation ($p_0 \ll p^*$) such that the chip is an ideal resistance. We do not expect the relaxation time to be pressure dependent in this limit. Conversely at high pressure, the deformation makes the resistance of the chip pressure dependent. According to Eq. 5, we have a chip resistance, and thus a timescale, that scales as $P_{0,\infty}^{-3}$. With these ideas in mind, we look for asymptotic, power-law solutions to Eq. 7, $\lambda_s \approx \beta^2\Pi^\gamma$, where β and γ are constants. Injecting such a solution into Eq. 7 and using asymptotic developments of the Bessel functions (Supplemental Material [45], section S.III), we confirm the aforementioned power laws, with

$$\frac{\tau_{\rm exp}}{\tau_c} = \frac{1}{\beta^2} \quad : \quad \Pi \ll 1 \ , \tag{9}$$

$$\frac{\tau_{\rm exp}}{\tau_c} = \frac{1}{\beta^2 P_{0,\infty}^3} \quad : \quad \Pi \gg 1 \ . \tag{10}$$

Here, β satifies $\mathcal{T}\beta^2 - \mathcal{R}\beta\cot(\beta) - 1 = 0$ and $\mathcal{T}\beta/\mathcal{R} = \mathrm{J}_{-1/5}(8\beta/5)/\mathrm{J}_{4/5}(8\beta/5)$ in the low- and high-Π limits; we note also that $\mathcal{T}$ and $\mathcal{R}$ may differ in these limits.

In order to obtain the smallest eigenvalue, λ_s, for intermediate pressures, Eq. 8 must be solved numerically for prescribed values of $\{\Pi, \mathcal{R}, \mathcal{T}\}$, thus necessitating characterisations of the input r_0 and c_0. Our input resistance was determined by measuring $p_{\mathrm{in},\infty}$ versus q_∞ in the presence of the flow meter only. The data (see Supplemental Material [45], section S.IV) are well described by a straight line, from which we obtain $r_0 = 2.50 \pm 0.01$ kPa s/nL, consistent with a rigid glass capillary of diameter 25 µm and length 2.4 cm filled with water of viscosity $\eta = 1.0$ mPa s [48]. The value of c_0 is assessed by plugging the circuit at the pressure sensor outlet and removing the microchannel, assuming that the resulting relaxation time satisfies $\tau_0 = r_0 c_0$. The inset of Fig. 4 shows τ_0 as a function of $p_{0,\infty}$ for such a plugged experiment, indicating a clearly nonlinear inlet capacity.

Assuming that the capacity at the channel inlet is dominated by a compression/dilatation of trapped air, and using the ideal gas law, we estimate $c_0 = c_1(1 + p_{0,\infty}/p_{\rm atm})^{-2} + c_2$. Here $p_{\rm atm}$=101 kPa is the atmospheric pressure, $c_1 = \Omega_b/p_{\rm atm}$, and Ω_b is the trapped air volume at atmospheric pressure. The second term describes any other linear elasticity. The solid line in the inset provides an excellent fit using this ideal-gas dominated inlet capacity, with $c_1 = 20.9 \pm 0.1$ nL kPa^{-1} and $c_2 = 0.2 \pm 0.1$ nL kPa^{-1} $\ll c_1$. The value of c_1 corresponds to a resting gas volume of 2.1 µL, which compares reasonably to the internal volume of the pressure sensor of 7.5 µL as provided by the manufacturer.

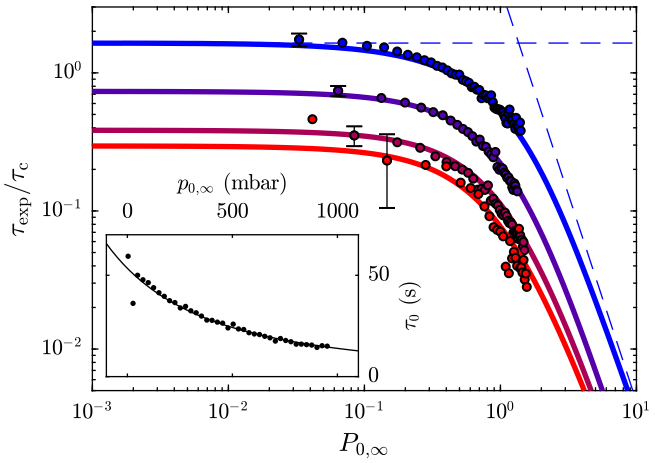

Figure 4. $\tau_{\rm exp}/\tau_c$ as a function of $P_{0,\infty}$ for four channels of different widths (the color map is the same as for Fig. 2). For clarity, a single, typical error bar is shown for each data set. Solid lines represent the numerical solution of the model of Eq. 8 and dashed lines are the asymptotic developments, shown only for the 200 µm-wide channel. The inset shows τ_0 as a function of $p_{0,\infty}$ for the plugged experiment. Error bars are smaller than symbol size. The solid line is a fit to the model including an ideal gas capacitance.

Making a full test of the model for our complete microfluidic system, Figure 4 shows the normalized relaxation time $\tau_{\rm exp}/\tau_c$ as a function of $P_{0,\infty}$ for all channel widths used here. The solid lines represent the numerical solution of the problem (Eqs. 7 and 8), where Eq. 7 is solved numerically using the aforementioned ideal resistance value and the ideal-gas, pressure-dependent capacitance. For this data the best-fitting values for c_1 and c_2 were 8.6 ± 0.4 and 2.1 ± 0.2 nL kPa^{-1}, respectively. Here the larger value of c_1 corresponds well to the linear capacity of the channel inlet, approximated by $c_2 \approx d_c^3/E^* \approx 1$ nL kPa^{-1}. We additionally show the asymptotic behaviors, where the equations for prefactors β were solved graphically using the limiting values of $\mathcal{T}$ and $\mathcal{R}$. Our model describes the data well over more than one decade of normalized pressures and for four chip geometries all fitted using the same c_1 and c_2, the experiments having been performed sequentially.

In conclusion, we have used time-resolved pressure and flow-rate measurements to characterize the relaxation dynamics of compliant microfluidic channels. First, we recover the well-documented, quartic pressure-*vs.*-flow-rate

relation for straight, rectangular channels. Additionally, we measured a full series of pressure-dependent relaxation time scales resulting from step-wise pressure perturbations in a series of chip widths, keeping the length and height of our chips constant. The nontrivial pressure-dependent relaxation rate is in accordance with our theoretical model, this latter based on a perturbation analysis of the lubrication-approximated microflow problem of a straight microfluidic channel. Such a lubrication analysis couples to a linear elasticity of the channel walls, and accounts fully for the the resistance and capacity effects of the previously-unconsidered, yet experimentally ubiquitous, microfluidic input peripheries. In a more general context, ours is a simple unit of many potential compliant flow networks, and our analysis thus could be applicable to a broad range of micro-biological, and micro-technological applications already finding applications but hitherto quantitatively characterized.

The authors thank Ivan C. Christov, Thomas Salez, Stéphane Jouenne and Andreas Carlson for fruitful discussions. The authors benefited from the financial support of the Agence Nationale de la Recherche (ANR) under the CoPinS (ANR-19CE06-0021) grants, and of the Institut Pierre-Gilles de Gennes (Equipex ANR-10-EQPX-34 and Labex ANR-10-LABX-31), PSL Research University (Idex ANR-10-IDEX-0001-02). Total Energies is also gratefully acknowledged for financial support under contract TOTAL DS3700 – CNRS 2019200804.

* joshua.mcgraw@cnrs.fr

[1] I. C. Christov, Journal of Physics: Condensed Matter **34**, 063001 (2021).
[2] T. Gervais, J. El-Ali, A. Günther, and K. F. Jensen, Lab on a Chip **6**, 500 (2006).
[3] I. C. Christov, V. Cognet, T. C. Shidhore, and H. A. Stone, Journal of Fluid Mechanics **841**, 267 (2018).
[4] R. Stribeck, *Kugellager für beliebige Belastungen* (Springer, 1901).
[5] R. Gohar and A. Cameron, Nature **200**, 458 (1963).
[6] K. Johnson, J. Greenwood, and S. Poon, Wear **19**, 91 (1972).
[7] J. Hansen, M. Björling, and R. Larsson, Scientific Reports **10**, 22250 (2020).
[8] S. Leroy and E. Charlaix, Journal of Fluid Mechanics **674**, 389 (2011).
[9] Y. Wang, C. Dhong, and J. Frechette, Physical review letters **115**, 248302 (2015).
[10] B. Saintyves, T. Jules, T. Salez, and L. Mahadevan, Proceedings of the National Academy of Sciences **113**, 5847 (2016).
[11] Z. Zhang, V. Bertin, M. Arshad, E. Raphaël, T. Salez, and A. Maali, Phys. Rev. Lett. **124**, 054502 (2020).
[12] V. Bertin, Y. Amarouchene, E. Raphaël, and T. Salez, Journal of Fluid Mechanics **933**, A23 (2022).
[13] S. Jahn, J. Seror, and J. Klein, Annual Review of Biomedical Engineering **18**, 235 (2016).
[14] M. Jones, G. Fulford, C. Please, D. McElwain, and M. J. Collins, Bulletin of Mathematical Biology **70**, 323 (2008).
[15] K. Perktold and G. Rappitsch, Journal of biomechanics **28**, 845 (1995).
[16] C. A. Figueroa, I. E. Vignon-Clementel, K. E. Jansen, T. J. Hughes, and C. A. Taylor, Computer methods in applied mechanics and engineering **195**, 5685 (2006).
[17] M. Heil and A. L. Hazel, Annual review of fluid mechanics **43**, 141 (2011).
[18] M. Hirschhorn, V. Tchantchaleishvili, R. Stevens, J. Rossano, and A. Throckmorton, Medical engineering & physics **78**, 1 (2020).
[19] C. A. Taylor, T. J. Hughes, and C. K. Zarins, Annals of biomedical engineering **26**, 975 (1998).
[20] H. S. Davies, D. Débarre, N. El Amri, C. Verdier, R. P. Richter, and L. Bureau, Physical review letters **120**, 198001 (2018).
[21] J. M. Skotheim and L. Mahadevan, Phys. Rev. Lett. **92**, 245509 (2004).
[22] H. Xia, J. Wu, J. Zheng, J. Zhang, and Z. Wang, Lab on a Chip **21**, 1241 (2021).
[23] Y. Xia and G. M. Whitesides, Annual Review of Materials Science **28**, 153 (1998).
[24] K. Raj M and S. Chakraborty, Journal of Applied Polymer Science **137**, 48958 (2020).
[25] D. Huh, B. D. Matthews, A. Mammoto, M. Montoya-Zavala, H. Y. Hsin, and D. E. Ingber, Science **328**, 1662 (2010).
[26] J. U. Lind, T. A. Busbee, A. D. Valentine, F. S. Pasqualini, H. Yuan, M. Yadid, S.-J. Park, A. Kotikian, A. P. Nesmith, P. H. Campbell, *et al.*, Nature materials **16**, 303 (2017).
[27] S. Xu, Y. Zhang, L. Jia, K. E. Mathewson, K.-I. Jang, J. Kim, H. Fu, X. Huang, P. Chava, R. Wang, *et al.*, Science **344**, 70 (2014).
[28] J. C. Yeo, C. T. Lim, *et al.*, Lab on a Chip **16**, 4082 (2016).
[29] D. P. Holmes, B. Tavakol, G. Froehlicher, and H. A. Stone, Soft Matter **9**, 7049 (2013).
[30] F. J. Meigel, P. Cha, M. P. Brenner, and K. Alim, Physical Review Letters **123**, 228103 (2019).
[31] E. Virot, V. Spandan, L. Niu, W. M. Van Rees, and L. Mahadevan, Physical Review Letters **125**, 058102 (2020).
[32] J. W. Rocks, A. J. Liu, and E. Katifori, Physical Review Letters **126**, 028102 (2021).
[33] K. Park, A. Tixier, M. Paludan, E. Østergaard, M. Zwieniecki, and K. H. Jensen, Phys. Rev. Fluids **6**, 123102 (2021).
[34] B. Mosadegh, C.-H. Kuo, Y.-C. Tung, Y.-s. Torisawa, T. Bersano-Begey, H. Tavana, and S. Takayama, Nature physics **6**, 433 (2010).
[35] J. A. Weaver, J. Melin, D. Stark, S. R. Quake, and M. A. Horowitz, Nature Physics **6**, 218 (2010).
[36] P. N. Duncan, T. V. Nguyen, and E. E. Hui, Proceedings of the National Academy of Sciences **110**, 18104 (2013).
[37] D. C. Leslie, C. J. Easley, E. Seker, J. M. Karlinsey, M. Utz, M. R. Begley, and J. P. Landers, Nature Physics **5**, 231 (2009).
[38] K. W. Oh, K. Lee, B. Ahn, and E. P. Furlani, Lab on a Chip **12**, 515 (2012).
[39] D. J. Preston, P. Rothemund, H. J. Jiang, M. P. Nemitz, J. Rawson, Z. Suo, and G. M. Whitesides, Proceedings of the National Academy of Sciences **116**, 7750 (2019).

[40] Z. Jiao, J. Zhao, Z. Chao, Z. You, and J. Zhao, Microfluidics and Nanofluidics **23**, 1 (2019).

[41] D. Dendukuri, S. S. Gu, D. C. Pregibon, T. A. Hatton, and P. S. Doyle, Lab Chip **7**, 818 (2007).

[42] X. Wang and I. C. Christov, Proceedings of the Royal Society A: Mathematical, Physical and Engineering Sciences **475**, 20190513 (2019).

[43] Y. Xia and G. M. Whitesides, Angewandte Chemie International Edition **37**, 550 (1998).

[44] The supplementary material contains a selection of raw data for the time-dependence of flow rate and pressures; asymptotic analysis of the eigenvalue equation; and flow sensor calibration data, see [URL to be input by the publisher] .

[45] See Supplemental Material at [URL will be inserted by publisher] for a selection of raw data for the time-dependence of flow rate and pressures; raw pressure-*vs*-flow-rate data; asymptotic analysis of the eigenvalue equation; and flow sensor calibration data.

[46] X. Wang and I. C. Christov, Physics of Fluids **33**, 102004 (2021).

[47] We note that the infinitely thick limit is expected when the thickness of the upper, flexible wall is roughly twice the width of the channel, which is always the case here. With the reported value [52] of ν=0.495, we have $E^* \approx 2.44 E_{\mathrm{Y}}$.

[48] H. Bruus, *Theoretical Microfluidics* (Oxford University Press, 2008).

[49] P. Tabeling, *Introduction to Microfluidics*, 1st ed. (Oxford University Press, 2010).

[50] A. Oron, S. H. Davis, and S. G. Bankoff, Reviews of modern physics **69**, 931 (1997).

[51] DLMF, "*NIST Digital Library of Mathematical Functions*," http://dlmf.nist.gov/, Release 1.1.5 of 2022-03-15, f. W. J. Olver, A. B. Olde Daalhuis, D. W. Lozier, B. I. Schneider, R. F. Boisvert, C. W. Clark, B. R. Miller, B. V. Saunders, H. S. Cohl, and M. A. McClain, eds.

[52] A. Müller, M. C. Wapler, and U. Wallrabe, Soft Matter **15**, 779 (2019).